Stable vortex and dipole vector solitons in a saturable nonlinear medium

Jianke Yang[1] and Dmitry E. Pelinovsky[2]
[1]*Department of Mathematics and Statistics, University of Vermont, Burlington, Vermont 05401*
[2]*Department of Mathematics, McMaster University, Hamilton, Ontario, Canada L8S 4K1*
(Received 17 September 2002; published 24 January 2003)

We study both analytically and numerically the existence, uniqueness, and stability of vortex and dipole vector solitons in a saturable nonlinear medium in $(2+1)$ dimensions. We construct perturbation series expansions for the vortex and dipole vector solitons near the bifurcation point, where the vortex and dipole components are *small*. We show that both solutions uniquely bifurcate from the same bifurcation point. We also prove that both vortex and dipole vector solitons are linearly *stable* in the neighborhood of the bifurcation point. Far from the bifurcation point, the family of vortex solitons becomes linearly unstable via oscillatory instabilities, while the family of dipole solitons remains stable in the entire domain of existence. In addition, we show that an unstable vortex soliton breaks up either into a rotating dipole soliton or into two rotating fundamental solitons.

DOI: 10.1103/PhysRevE.67.016608 PACS number(s): 42.65.Tg, 05.45.Yv

I. INTRODUCTION

Spatial solitons have been a subject of many studies since their first theoretical prediction [1]. The previous research on spatial solitons was driven by their promising applications in all-optical devices, in which the light guides and steers the light itself [2]. Early works studied optical materials with the Kerr (cubic) nonlinearity, which exhibit stable fundamental (single-hump) solitons in one spatial dimension [3–5] and collapse in two and three spatial dimensions [6,7]. Later works focused on optical materials with saturable nonlinear response such as photorefractive crystals (see Ref. [8], and references therein). The nonlinearity saturation suppresses the collapse of fundamental solitons in two and three dimensions [9–11], which opens the door for their experimental observation in multidimensional optical beams. The instability of higher-order (multihump) solitons is, however, not suppressed by the nonlinearity saturation [12–16]. Internal modes of fundamental solitons in saturable optical materials have also been reported [16,17]. These modes are responsible for long-lived shape oscillations.

Recently, incoherent coupling of spatial solitons in photorefractive crystals was proposed and experimentally demonstrated [11,18]. The mutual trapping of incoherent optical beams leads to many novel spatial solitons such as vortex and dipole vector solitons [19–28]. The incoherently coupled spatial solitons are described by a system of coupled nonlinear Schrödinger (NLS) equations. A similar system of equations also describes temporal solitons in birefringent optical fibers and wavelength-division-multiplexed systems [29–34]. Additionally, vortex vector solitons are known in the Bose-Einstein condensation guided by a magnetic trap [35].

Vortex and dipole vector solitons in saturable optical materials are interesting for both physical and mathematical reasons. Physically, these spatial solitons are novel nonlinear objects. They bifurcate from a coupled state, where a fundamental soliton in one component guides a small higher-order mode in the other component. Far from the bifurcation threshold, both components strongly trap each other and form a fully coupled vector soliton. Mathematically, existence and stability of the vortex and dipole vector solitons are challenging problems due to their complexity. The existence of vortex and dipole solitons was established numerically [20,23] and with a heuristic variational method [28]. However, analytical expressions for radial-angular dependences of vortex and dipole solitons have not been found. On the stability of vortex solitons, the numerical results of Ref. [20] suggest that vortex solitons with *small* vortex components are stable and observable for large propagation distances, while vortex solitons with large vortex components are unstable. Numerical results of Ref. [23] show, however, that *all* vortex solitons are linearly unstable, and the instability leads to the breakup of vortex solitons into rotating dipole solitons. The discrepancy between Refs. [20] and [23] raises an open question: are vortex vector solitons with small vortex components really stable or not? On the other hand, dipole solitons were found numerically to be always stable in Ref. [23].

In this paper, we clarify the issues of existence and stability of vortex and dipole vector solitons in a saturable nonlinear medium such as photorefractive crystals. First, we address the existence and uniqueness of vortex and dipole solitons with the perturbation technique [36,37]. We derive perturbation series expansions for the vortex and dipole solitons near the bifurcation point, where the vortex and dipole components are *small*. The analytical formulas for these solitons are in an excellent agreement with our numerical results. We also prove that those vector solitons are unique up to phase, translation, and rotation invariances. Next, we study the linear stability of vortex and dipole solitons with both the spectral analysis and numerical methods. We show that dipole solitons are linearly stable in the entire existence domain, while the vortex solitons with *large* vortex components are linearly unstable, in agreement with Ref. [23]. However, we prove that vortex solitons with *small* vortex components are linearly *stable*, confirming the results of Ref. [20], not Ref. [23]. Lastly, we study the nonlinear evolution of linearly unstable vortex solitons. We show that an unstable vortex soliton breaks up into a rotating dipole soliton only when the vortex component is below a certain threshold.

Above this threshold, an unstable vortex soliton breaks up into two fundamental vector solitons instead.

II. EXISTENCE AND UNIQUENESS OF VORTEX AND DIPOLE SOLITONS

The mathematical model for two incoherently coupled laser beams in a photorefractive crystal is well known (see, e.g., Refs. [20,23]). After variable rescalings, the model can be written as a system of coupled equations,

$$i\frac{\partial E_1}{\partial z}+\Delta E_1+\frac{E_1(|E_1|^2+|E_2|^2)}{1+s(|E_1|^2+|E_2|^2)}=0, \tag{1}$$

$$i\frac{\partial E_2}{\partial z}+\Delta E_2+\frac{E_2(|E_1|^2+|E_2|^2)}{1+s(|E_1|^2+|E_2|^2)}=0, \tag{2}$$

where Δ is the two-dimensional Laplacian, and s is the saturation parameter.

Vector solitons in this model take the form

$$E_1=u(x,y)e^{iz}, \quad E_2=w(x,y)e^{i\lambda z}, \tag{3}$$

where the frequency of the E_1 wave has been normalized to one, and the frequency of the E_2 wave is λ. The amplitude functions $u(x,y)$ and $w(x,y)$ satisfy the nonlinear boundary-value problem with zero boundary conditions on the (x,y) plane:

$$\Delta u-u+\frac{u(|u|^2+|w|^2)}{1+s(|u|^2+|w|^2)}=0, \tag{4}$$

$$\Delta w-\lambda w+\frac{w(|u|^2+|w|^2)}{1+s(|u|^2+|w|^2)}=0. \tag{5}$$

The systems (4) and (5) may have several types of vector solitons localized in two dimensions. The *fundamental* vector solitons take the form

$$u=c_u\Phi(r), \quad w=c_w\Phi(r), \tag{6}$$

where $\Phi(r)$ is a real-valued, single-hump function, $r=\sqrt{x^2+y^2}$, and c_u and c_w are arbitrary complex parameters constrained by the relation $|c_u|^2+|c_w|^2=1$. These solitons exist at $\lambda=1$, where the systems (4) and (5) reduce to a scalar equation for $\Phi(r)$, see Eq. (10) below. The *vortex* vector solitons take a general form

$$u=\Phi_u(r)e^{in\theta}, \quad w=\Phi_w(r)e^{im\theta}, \tag{7}$$

where n and m are topological charges of vortices in the u and w components, $\Phi_u(r)$ and $\Phi_w(r)$ are real-valued functions, and (r,θ) are the polar coordinates on the (x,y) plane. The simplest vortex soliton has $n=0$ and $m=1$ [20,23]. The *multipole* vector solitons take yet another general form

$$u=U(r,\theta), \quad w=W(r,\theta), \tag{8}$$

where $U(r,\theta)$ and $W(r,\theta)$ are real-valued functions and may have multihump profiles on the (x,y) plane. The multipole solitons with a single hump for $u(x,y)$ and multiple humps for $w(x,y)$ were approximated in the variational approach [28] by the ansatz,

$$u=U(r), \quad w=W(r)\cos m\theta, \tag{9}$$

where the number of humps in the w component is $2m$. The simplest multipole soliton is a dipole soliton, which has $m=1$.

In this paper, we study the simplest vortex and multipole vector solitons. We will refer to them simply as the vortex soliton and dipole soliton, hereafter. The existence and uniqueness of the vortex and dipole solitons can be studied by perturbation methods. The perturbation series expansions are derived in the neighborhood of the bifurcation value $\lambda=\lambda_0(s)$, where the w component is small. With the perturbation arguments, we show that the bifurcation value $\lambda_0(s)$ is the same for both branches of vortex and dipole solitons, and these solitons bifurcate uniquely from $\lambda=\lambda_0(s)$.

Setting $w=0$ in Eq. (4), we find the nonlinear boundary-value problem for the scalar soliton $u=u_0(r)$,

$$u_0''+\frac{1}{r}u_0'-u_0+\frac{u_0^3}{1+su_0^2}=0, \tag{10}$$

where $u_0(r)$ is a real-valued function. We take $u_0(r)$ to be the fundamental soliton, i.e., $u_0(r)>0$ for finite $r\geqslant 0$. When w is small in Eq. (5), we get a linear eigenvalue problem for the first-order correction $w=w_1(x,y)$,

$$\Delta w_1-\lambda w_1+\frac{u_0^2}{1+su_0^2}w_1=0, \tag{11}$$

where $w_1(x,y)$ is a complex-valued function, in general, and λ is the eigenvalue. The linear equation (11) supports localized solutions of the form $\phi(r)e^{\pm im\theta}$ for some discrete values of λ. Since, we study the simplest vortex and dipole solitons, we set $m=1$, and require $\phi(r)$ to be a non-negative function for $r\geqslant 0$. The corresponding eigenvalue $\lambda_0(s)$ and eigenfunction $\phi(r)$ satisfy the following reduced equation:

$$\phi''+\frac{1}{r}\phi'-\left(\lambda_0+\frac{1}{r^2}\right)\phi+\frac{u_0^2}{1+su_0^2}\phi=0. \tag{12}$$

The eigenvalue λ_0 is unique once s is fixed. We normalize the eigenfunction $\phi(r)$ such that it has a maximum value one. Numerically, we compute $\lambda_0(s)$ and $\phi(r)$ by the shooting method. Figure 1(a) shows the dependence of λ_0 versus

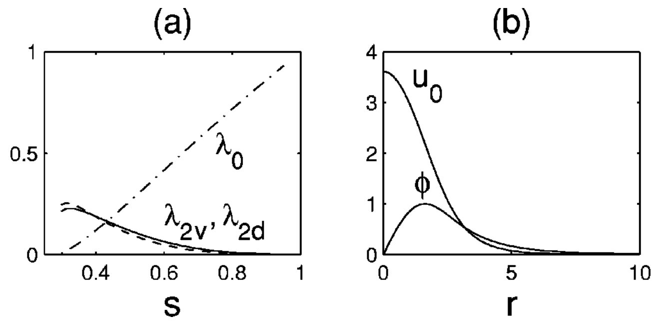

FIG. 1. (a) The cutoff frequency λ_0 (dashed-dotted) and the correction terms λ_{2v} (dashed) and λ_{2d} (solid) for vortex and dipole solitons as a function of s. (b) The scalar $u_0(r)$ soliton and the normalized eigenfunction $\phi(r)$ at $s=0.5$.

saturation parameter s. Figure 1(b) shows the scalar soliton $u_0(r)$ and the normalized eigenfunction $\phi(r)$ at $s=0.5$, where $\lambda_0=0.2622$.

When $\phi(r)$ and $\lambda_0(s)$ are known, a general solution for $w_1(r,\theta)$ can be written in the form

$$w_1(r,\theta)=\phi(r)(\cos\theta+ip\sin\theta), \tag{13}$$

where p is an arbitrary real parameter. In this general solution, we have removed arbitrary rotations and translations on the (x,y) plane as well as an arbitrary phase shift in the w component. We note that the solution (13) is identical to the variational ansatz in Ref. [28].

Below, we use the perturbative method and show that there are only two continuations of the solution (13): for $p=\pm 1$ and $p=0$. When $p=\pm 1$, the perturbation series expansion recovers the vortex soliton (7) with $n=0$ and $m=\pm 1$. When $p=0$, the perturbation expansion recovers the dipole soliton (8) with a single hump for u and a double hump for w. For given values of s and λ, the two solutions are unique up to phase, translation, and rotation invariances. At other values of p, the solution with w's leading-order term as in Eq. (13) cannot exist.

The perturbation series expansions for vector solitons in systems (4) and (5) take the form

$$u=u_0(r)+\epsilon^2 u_2(r,\theta)+\epsilon^4 u_4(r,\theta)+O(\epsilon^6), \tag{14}$$

$$w=\epsilon w_1(r,\theta)+\epsilon^3 w_3(r,\theta)+\epsilon^5 w_5(r,\theta)+O(\epsilon^7), \tag{15}$$

and

$$\lambda=\lambda_0(s)+\epsilon^2\lambda_2(s)+\epsilon^4\lambda_4(s)+O(\epsilon^6), \tag{16}$$

where ϵ is a small parameter, $u_0(r)$ is the scalar fundamental soliton solving Eq. (10), $w_1(r,\theta)$ is the first-order correction in the form (13), and the cutoff frequency λ_0 is the eigenvalue of Eq. (12). The objective of the perturbation analysis is to uniquely determine the coefficients $\lambda_2,\lambda_4,\ldots$ as well as expressions for functions u_2, u_4, w_3,w_5, and so on. Once the coefficients $\lambda_0,\lambda_2,\ldots$ have been obtained, we can compute ϵ from λ in the expansion (16). Once ϵ is found, together with functions $u_0,u_2,w_1,w_3,\ldots$, we can approximate the vector soliton by the expansions (14) and (15). Below, we will carry out the perturbative calculations to the order of ϵ^3.

Substituting the perturbation series (14), (15), and (16) into the original Eqs. (4) and (5), at order ϵ^2, we get an inhomogeneous equation for u_2,

$$\Delta u_2-u_2+\frac{u_0^2(2+su_0^2)}{(1+su_0^2)^2}u_2+\frac{u_0^2}{(1+su_0^2)^2}\overline{u}_2=-\frac{u_0|w_1|^2}{(1+su_0^2)^2}, \tag{17}$$

where $\overline{u}$ is the complex conjugate of u. The linearized operator in the left-hand side of Eq. (17) has a nonempty null space spanned by three linearly independent localized eigenfunctions

$$u_{2h}^{(1)}=iu_0(r),\quad u_{2h}^{(2)}=u_0'(r)\cos\theta,\quad u_{2h}^{(3)}=u_0'(r)\sin\theta. \tag{18}$$

These eigenfunctions correspond to the phase and translational invariances of solitons in the scalar u equation. The right-hand side of Eq. (17) is orthogonal to $u_{2h}^{(1)}$ because it is real valued. It is also orthogonal to $u_{2h}^{(2)}$ and $u_{2h}^{(3)}$ because it has different angular dependence of 1 and $\cos 2\theta$ (rather than $\cos\theta$ and $\sin\theta$). Therefore, up to phase, translation, and rotation shifts, a localized solution to Eq. (17) is constructed uniquely in the form

$$u_2=\frac{1}{2}(1+p^2)u_{20}(r)+\frac{1}{2}(1-p^2)u_{22}(r)\cos 2\theta, \tag{19}$$

where functions $u_{20}(r)$ and $u_{22}(r)$ satisfy the equations

$$u_{20}''+\frac{1}{r}u_{20}'-u_{20}+\frac{u_0^2(3+su_0^2)}{(1+su_0^2)^2}u_{20}=-\frac{u_0\phi^2}{(1+su_0^2)^2}, \tag{20}$$

$$u_{22}''+\frac{1}{r}u_{22}'-\left(1+\frac{4}{r^2}\right)u_{22}+\frac{u_0^2(3+su_0^2)}{(1+su_0^2)^2}u_{22}=-\frac{u_0\phi^2}{(1+su_0^2)^2}. \tag{21}$$

We do not know exact analytical expressions for $u_{20}(r)$ and $u_{22}(r)$ but can compute them numerically.

At order ϵ^3, we get the equation for w_3 as

$$\Delta w_3-\lambda_0 w_3+\frac{u_0^2}{1+su_0^2}w_3=\left\{\lambda_2-\frac{|w_1|^2+2u_0u_2}{(1+su_0^2)^2}\right\}w_1. \tag{22}$$

We denote

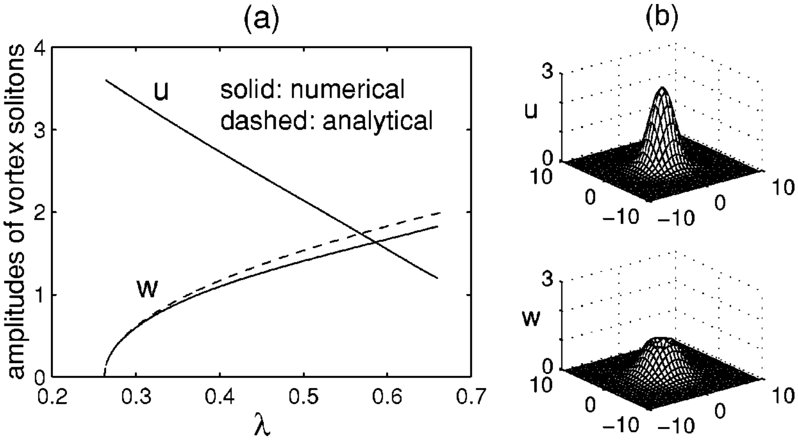

FIG. 2. (a) Amplitudes of the vortex vector solitons obtained analytically (dashed line) and numerically (solid line) for $s=0.5$ and various frequencies λ. (b) A numerical vortex-soliton solution with $s=0.5$ and $\lambda=0.4$.

$$h_1(r)=\frac{\phi^2+2u_0u_{20}}{2(1+su_0^2)^2}, \quad h_2(r)=\frac{\phi^2+2u_0u_{22}}{2(1+su_0^2)^2}, \tag{23}$$

and rewrite Eq. (22) in the form

$$\begin{aligned}\Delta w_3-\lambda_0 w_3+\frac{u_0^2}{1+su_0^2}w_3 \\ =\left[\lambda_2-(1+p^2)h_1-\frac{1}{2}(1-p^2)h_2\right]\phi\cos\theta \\ +ip\left[\lambda_2-(1+p^2)h_1+\frac{1}{2}(1-p^2)h_2\right]\phi\sin\theta \\ -\frac{1}{2}(1-p^2)h_2\phi\cos 3\theta \\ -\frac{1}{2}ip(1-p^2)h_2\phi\sin 3\theta.\end{aligned} \tag{24}$$

The homogeneous part in Eq. (24) supports two linearly independent localized solutions $\phi(r)\cos\theta$ and $\phi(r)\sin\theta$. As a result, a localized solution of the nonhomogeneous Eq. (24) exists if and only if the following solvability conditions are satisfied:

$$\int_0^\infty r\phi^2\left\{\lambda_2-(1+p^2)h_1(r)-\frac{1}{2}(1-p^2)h_2(r)\right\}dr=0, \tag{25}$$

$$p\int_0^\infty r\phi^2\left\{\lambda_2-(1+p^2)h_1(r)+\frac{1}{2}(1-p^2)h_2(r)\right\}dr=0. \tag{26}$$

We will show below that these solvability conditions define only two perturbation series solutions for vector solitons. These solutions correspond to the choice $p=\pm 1$ or $p=0$, which produce vortex and dipole solitons, respectively.

A. Vortex solitons

If $p\neq 0$, we eliminate parameter λ_2 from the systems (25) and (26) and find the solvability condition in the form:

$$(1-p^2)\int_0^\infty r\phi^2 h_2(r)dr=0. \tag{27}$$

The integral in Eq. (27) only depends on the parameter s, not on p. We have checked numerically that this integral never vanishes for any s. Thus, the condition (27) is satisfied only when $p=\pm 1$. In this case, it follows from Eqs. (13), (19), and (24) that $w_1=\phi(r)e^{\pm i\theta}$, $u_2=u_{20}(r)$, and $w_3=f(r)e^{\pm i\theta}$. We can continue the perturbation series expansions (14)–(16) to higher orders and find that all u_{2n} ($n\geqslant 0$) corrections are only functions of r, and all w_{2n+1} ($n\geqslant 0$) corrections have the form $g(r)e^{\pm i\theta}$. Thus, the perturbation series solution gives a vortex vector soliton (7) with $n=0$ and $m=\pm 1$.

When $p=\pm 1$, we find from Eq. (25) that the coefficient λ_2 is

$$\lambda_2=\lambda_{2v}(s)\equiv\frac{2\int_0^\infty r\phi^2 h_1 dr}{\int_0^\infty r\phi^2 dr}. \tag{28}$$

The functional dependence of λ_{2v} versus s is computed from this formula and plotted in Fig. 1(a) (dashed line) alongside the cutoff frequency $\lambda_0(s)$. Since the (non-negative) function $\phi(r)$ is normalized to have a maximum one, the perturbation parameter ϵ determines the amplitude (maximum) of the vortex component w with error at the order of ϵ^3, see Eqs. (13) and (15). The dependence of ϵ versus λ and s can be obtained from the perturbation series (16) with an error of the order of ϵ^2:

$$\epsilon=\sqrt{\frac{\lambda-\lambda_0(s)}{\lambda_{2v}(s)}}. \tag{29}$$

We compare the analytical formula (29) with numerical results for $s=0.5$, where $\lambda_0=0.2622$ and $\lambda_{2v}=0.1010$. A dashed line in Fig. 2(a) shows the amplitude of the vortex component w computed from Eq. (29). Numerically, vortex solitons are computed from the original systems (4) and (5) by the shooting method. The amplitudes of the u and w components are also shown in Fig. 2. In Fig. 2(b), a profile of

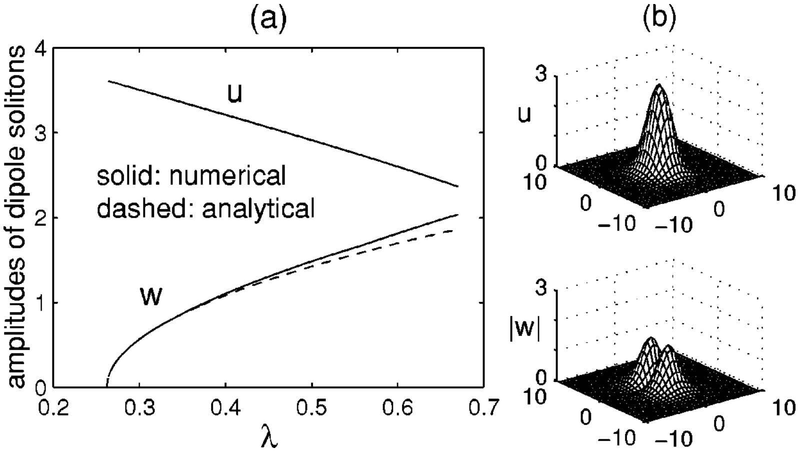

FIG. 3. (a) Amplitudes of the dipole vector solitons obtained analytically (dashed line) and numerically (solid line) for $s=0.5$ and various frequencies λ. (b) A numerical dipole-soliton solution with $s=0.5$ and $\lambda=0.5$.

$u(x,y)$ and $w(x,y)$ components for $s=0.5$ and $\lambda=0.4$ is shown. We can see from Fig. 2(a) that the agreement between the analytical predictions and numerical values on the amplitudes of the w component is good over a wide range of λ values. Also, the numerically obtained amplitude of the u component depends linearly on λ, which is in agreement with the perturbation series (14) up to an error of the order of ϵ^4, since $\epsilon^2 \propto (\lambda-\lambda_0)$.

B. Dipole solitons

If $p=0$, the condition (26) is satisfied, while the condition (25) gives the correction term λ_2 in the form

$$\lambda_2=\lambda_{2d}(s)\equiv\frac{\int_0^\infty r\phi^2(2h_1+h_2)dr}{2\int_0^\infty r\phi^2 dr}. \tag{30}$$

The functional dependence of λ_{2d} versus s is numerically computed and plotted in Fig. 1(a) (solid line). When λ_2 is given by Eq. (30), a localized solution $w_3(r,\theta)$ of Eq. (24) exists, and this solution is real valued. We can further show that the perturbation series expansions (14)–(16) can be successfully continued to higher orders of ϵ, and a dipole-soliton solution (8) can be obtained. This solution is real valued and has the symmetries

$$u(-x,y)=u(x,y),\quad u(x,-y)=u(x,y),$$

$$w(-x,y)=-w(x,y),\quad w(x,-y)=w(x,y). \tag{31}$$

Similar to the vortex soliton case, the perturbation parameter ϵ here gives the amplitude (maximum) of the dipole component w with accuracy of $O(\epsilon^3)$. The formula for ϵ is still Eq. (29), but the λ_2 value is now given by Eq. (30) instead of Eq. (28). The comparison between the analytical results (29) and (30) and numerical results for dipole solitons is shown in Fig. 3(a) for $s=0.5$. In this case, $\lambda_0=0.2622$ and $\lambda_{2d}=0.1174$. We see again that the agreement between numerical and analytical results is very good over a wide range of λ values. In Fig. 3(b), the profiles of $u(x,y)$ and $w(x,y)$ components of a dipole soliton, computed with numerical iteration methods, are displayed.

We note that in view of Eqs. (28) and (30), the integral in Eq. (27) is actually

$$\int_0^\infty r\phi^2 h_2(r)dr=(2\lambda_{2d}-\lambda_{2v})\int_0^\infty r\phi^2 dr. \tag{32}$$

Inspection of the $\lambda_{2d}(s)$ and $\lambda_{2v}(s)$ curves in Fig. 1(a) immediately confirms that the integral (32) is always positive. Thus, Eq. (27) holds only when $p=\pm 1$.

To summarize, we have shown that there are only two vector solitons of the systems (4) and (5), which bifurcate from the cutoff frequency $\lambda=\lambda_0(s)$. They are either a vortex soliton (7) or a real-valued dipole soliton (8). The solutions are determined in terms of perturbation series expansions up to the order of ϵ^3. Both solitons are unique up to phase, position, and rotation invariances. The analytical results are confirmed by numerical calculations. Computations of the perturbation series expansions prove the existence and uniqueness of vortex and dipole vector solitons observed numerically in Refs. [20,23,28].

III. LINEAR STABILITY OF VORTEX AND DIPOLE SOLITONS

In this section, we study the linear stability of vortex and dipole vector solitons by spectral analysis, supplemented by numerical computations. Since the linearization operators differ for vortex and dipole solitons, we shall treat the two cases separately.

A. Vortex solitons

To study the linear stability of the vortex solitons (7) with $n=0$ and $m=1$, we linearize the system (1) and (2) with the perturbation in the form

$$E_1=e^{iz}[\Phi_u(r)+u_+(r)e^{-in\theta+\sigma z}+\overline{u_-}(r)e^{in\theta+\overline{\sigma}z}], \tag{33}$$

$$E_2=e^{i\lambda z+i\theta}[\Phi_w(r)+w_+(r)e^{-in\theta+\sigma z}+\overline{w_-}(r)e^{in\theta+\overline{\sigma}z}]. \tag{34}$$

The linearization problem can be written in the form

$$i\sigma u_{+}=-u_{+}''-\frac{1}{r}u_{+}'+\left(1+\frac{n^{2}}{r^{2}}\right)u_{+}-Vu_{+}-V_{uu}(u_{+}+u_{-})-V_{uw}(w_{+}+w_{-}), \tag{35}$$

$$-i\sigma u_{-}=-u_{-}''-\frac{1}{r}u_{-}'+\left(1+\frac{n^{2}}{r^{2}}\right)u_{-}-Vu_{-}-V_{uu}(u_{+}+u_{-})-V_{uw}(w_{+}+w_{-}), \tag{36}$$

$$i\sigma w_{+}=-w_{+}''-\frac{1}{r}w_{+}'+\left(\lambda+\frac{(n-1)^{2}}{r^{2}}\right)w_{+}-Vw_{+}-V_{uw}(u_{+}+u_{-})-V_{ww}(w_{+}+w_{-}), \tag{37}$$

$$-i\sigma w_{-}=-w_{-}''-\frac{1}{r}w_{-}'+\left(\lambda+\frac{(n+1)^{2}}{r^{2}}\right)w_{-}-Vw_{-}-V_{uw}(u_{+}+u_{-})-V_{ww}(w_{+}+w_{-}), \tag{38}$$

where

$$V=\frac{\Phi_u^2+\Phi_w^2}{1+s(\Phi_u^2+\Phi_w^2)},\quad V_{uu}=\frac{\Phi_u^2}{[1+s(\Phi_u^2+\Phi_w^2)]^2},$$

$$V_{uw}=\frac{\Phi_u\Phi_w}{[1+s(\Phi_u^2+\Phi_w^2)]^2},\quad V_{ww}=\frac{\Phi_w^2}{[1+s(\Phi_u^2+\Phi_w^2)]^2}.$$

The linearized problem can be formulated in the Hamiltonian form [35]:

$$\pm i\sigma u_{\pm}=\frac{\delta h}{\delta \overline{u}_{\pm}},\quad \pm i\sigma w_{\pm}=\frac{\delta h}{\delta \overline{w}_{\pm}}, \tag{39}$$

where h is the energy quadratic form associated with an eigenvector $\mathbf{u}=(u_+,u_-,w_+,w_-)^T$ and a linearized self-adjoint operator $\mathcal{L}$ of the right-hand sides of the system (35)–(38):

$$h=\langle \mathbf{u},\mathcal{L}\mathbf{u}\rangle=i\sigma\int_0^\infty r\,dr(|u_+|^2-|u_-|^2+|w_+|^2-|w_-|^2). \tag{40}$$

The eigenvalue σ is defined by the spectrum of the linearized problem (35)–(38) when $\mathbf{u}(r)$ is localized as $r\to\infty$ such that the integral (40) makes sense. The eigenvalues could be isolated or embedded into a continuous spectrum of the system (35)–(38). The vortex soliton is linearly unstable if there exists an eigenvalue σ for some n such that $\mathrm{Re}(\sigma)>0$. We note that if $(\sigma,n,u_+,u_-,w_+,w_-)$ is a solution of the linear system (35)–(38), so are $(\overline{\sigma},-n,\overline{u}_-,\overline{u}_+,\overline{w}_-,\overline{w}_+)$, $(-\sigma,-n,u_-,u_+,w_-,w_+)$, and $(-\overline{\sigma},n,\overline{u}_+,\overline{u}_-,\overline{w}_+,\overline{w}_-)$. Thus, complex unstable eigenvalues σ always come in quartets, while real and imaginary eigenvalues σ always come in pairs. We also note that eigenmodes $(\sigma,n,u_+,u_-,w_+,w_-)$ and $(\overline{\sigma},-n,\overline{u}_-,\overline{u}_+,\overline{w}_-,\overline{w}_+)$ give the identical perturbation in Eqs. (33) and (34), so do the eigenmodes $(-\sigma,-n,u_-,u_+,w_-,w_+)$ and $(-\overline{\sigma},n,\overline{u}_+,\overline{u}_-,\overline{w}_+,\overline{w}_-)$.

According to the stability theory of solitary waves in the system of coupled NLS equations [38], only eigenvalues σ with negative or zero values of the energy quadratic form (40) may bifurcate to the domain $\mathrm{Re}(\lambda)>0$, leading to instabilities. We shall apply this theory and study the spectrum of the linearization problem (35)–(38) at the cutoff frequency $\lambda=\lambda_0(s)$, where $\Phi_u(r)=u_0(r)$ and $\Phi_w(r)=0$. We will show that the vortex soliton is linearly stable in the neighborhood of the cutoff frequency $\lambda_0(s)\leqslant\lambda<\lambda_c(s)$, where $\lambda_c(s)\leqslant 1$ is the instability threshold. In the limit $\lambda\to\lambda_0(s)$, the linearization problem decomposes into two linear problems

$$\pm i\sigma u_{\pm}=-u_{\pm}''-\frac{1}{r}u_{\pm}'+\left(1+\frac{n^{2}}{r^{2}}\right)u_{\pm}-\frac{u_0^2}{1+su_0^2}u_{\pm}-\frac{u_0^2(u_++u_-)}{(1+su_0^2)^2}, \tag{41}$$

and

$$\pm i\sigma w_{\pm}=-w_{\pm}''-\frac{1}{r}w_{\pm}'+\left(\lambda_0+\frac{(n\mp1)^{2}}{r^{2}}\right)w_{\pm}-\frac{u_0^2}{1+su_0^2}w_{\pm}. \tag{42}$$

The first linear problem (41) is the stability problem of a scalar fundamental soliton $u=u_0(r)$ in a saturable medium. The linear stability of such solitons has been well established (see Ref. [16] for instance), thus unstable eigenvalues σ do not exist in Eq. (41). The continuous spectrum of the system (41) is located at $\mathrm{Re}(\sigma)=0$ and $|\mathrm{Im}(\sigma)|\geqslant 1$. The continuous spectrum is irrelevant for stability of solitary waves in the system of coupled NLS equations when no embedded eigenvalues with negative energy quadratic form (40) exist [38]. The discrete spectrum of Eq. (41) consists of isolated eigenvalues σ such that $\mathrm{Re}(\sigma)=0$ and $|\mathrm{Im}(\sigma)|<1$, including the zero eigenvalue at $n=0$ and $n=\pm1$ with three eigenfunctions (18) and three generalized eigenfunctions. Additional eigenvalues for internal modes exist in Eq. (41) for $\mathrm{Re}(\sigma)=0$ and $0\neq|\mathrm{Im}(\sigma)|<1$. These modes have been determined numerically in Ref. [16]. Using those numerical results, we have found that the energy quadratic form (40) is positive for all internal modes of the system (41). For instance, only one internal mode with $n=0$ exists and has positive value of h for $s=0.5$ (which corresponds to $\omega=-0.5$ in Ref. [16], see Fig. 3). We have also checked that no embedded eigenvalues with $|\mathrm{Im}(\sigma)|\geqslant 1$ exist in the problem (41) for $s=0.5$.

The second linear problem (42) is uncoupled for w_+ and w_-. Since the operator on the right-hand side of Eq. (42) is self-adjoint, the spectrum of σ is purely imaginary, i.e., $\mathrm{Re}(\sigma)=0$. The continuous spectrum of Eq. (42) is located at $|\mathrm{Im}(\sigma)|>\lambda_0$. Its discrete spectrum consists of isolated eigenvalues with $\mathrm{Im}(\sigma)>-\lambda_0$ for w_+ and $\mathrm{Im}(\sigma)<\lambda_0$ for w_- and can be embedded into a continuous spectrum. The discrete spectrum of Eq. (42) includes two zero eigenvalues at $n=0$ with eigenfunctions $w_\pm=\phi(r)$, two zero eigenvalues at $n=\pm 2$ with eigenfunctions $w_\pm=\phi(r)$, and two nonzero eigenvalues $\sigma=\pm i(1-\lambda_0)$ at $n=\pm 1$ with eigenfunctions $w_\pm=u_0(r)$. The zero eigenvalues at $n=0$ are induced by the phase invariance of the E_2 equation, while the zero eigenvalues at $n=\pm 2$ are induced by the symmetry of the uncoupled problem (42). The eigenvalues $\sigma=\pm i(1-\lambda_0)$ with $n=\pm 1$ are induced by the arbitrary polarizations in the fundamental vector soliton (6) at $\lambda=\lambda_0(s)$. The latter eigenvalues result in negative values of the energy quadratic form (40),

$$h=-(1-\lambda_0)\int_0^\infty u_0^2(r)r\,dr<0. \tag{43}$$

We have checked numerically that Eq. (42) has no other discrete eigenvalues for $s=0.5$.

Applying the stability theory of solitary waves [38], we count eigenvalues of the problems (41) and (42), which produce negative and zero values of the energy quadratic form h. At $\lambda=\lambda_0(s)$, only two eigenvalues $\sigma=\pm i(1-\lambda_0)$ give the negative energy (43). Several zero eigenvalues give zero energy at $n=0,\pm 1,\pm 2$. However, zero eigenvalues at $n=0$ and $n=\pm 1$ are preserved at $\lambda>\lambda_0(s)$ due to translation, rotation, and complex-phase symmetries of the systems (1) and (2). Only two zero eigenvalues of the problem (42) at $n=\pm 2$ are not preserved by the symmetry and they can move out of zero for $\lambda>\lambda_0(s)$. We shall now consider the shift of these negative-energy and zero-energy eigenvalues for λ near the cutoff frequency $\lambda_0(s)$.

We show first that the negative-energy eigenvalues $\sigma=\pm i(1-\lambda_0)$ never bifurcate off the imaginary axis for $\lambda>\lambda_0(s)$ regardless whether they are embedded or not. Indeed, at any value of λ, the linearization problems (35)–(38) have the exact discrete eigenmode

$$u_+=0,\quad u_-=-\Phi_w(r),\quad w_+=\Phi_u(r),\quad w_-=0 \tag{44}$$

for $n=1$ and $\sigma=i(1-\lambda)$, and

$$u_+=-\Phi_w(r),\quad u_-=0,\quad w_+=0,\quad w_-=\Phi_u(r) \tag{45}$$

for $n=-1$ and $\sigma=-i(1-\lambda)$. This result is in contrast with what happens in the system of coupled NLS equations with Kerr nonlinearities, where the negative-energy discrete eigenvalues, which are embedded in the continuous spectrum, bifurcate to the complex plane and lead to the instability [36,38].

We note that the exact eigenmodes (44) and (45) generate an approximate solution of the systems (1) and (2):

$$E_1=\Phi_u(r)e^{iz}-\gamma\Phi_w(r)e^{i\theta+i\lambda z}+O(\gamma^2),$$
$$E_2=\Phi_w(r)e^{i\theta+i\lambda z}+\gamma\Phi_u(r)e^{iz}+O(\gamma^2), \tag{46}$$

where γ is an arbitrary small parameter. Solution (46) is nothing but the original vortex vector soliton under a small rotation in the (E_1,E_2) plane. This rotation leaves the original systems (1) and (2) invariant, and is one of the symmetries of the present problem. Thus, although the solution (46) appears like internal oscillations of vortex solitons, this oscillation does not create any energy radiation and is fundamentally different from internal oscillations discussed in Refs. [16,17,36].

We show next that the zero eigenvalues at $n=\pm 2$ move to the imaginary axis (as conjugate pairs) as $\lambda>\lambda_0(s)$ and do not create any instability. We will use the perturbation series expansions and will present calculations only for the case $n=2$ (the case $n=-2$ is similar). When λ is close to $\lambda_0(s)$, we construct an approximate solution to the linearization problem (35)–(38) at $n=2$ in the form

$$u_\pm=\epsilon u_\pm^{(1)}(r)+O(\epsilon^3),\quad w_+=\phi(r)+\epsilon^2 w_+^{(2)}(r)+O(\epsilon^4),$$
$$w_-=\epsilon^2 w_-^{(2)}(r)+O(\epsilon^4),\quad \sigma=\epsilon^2\sigma_2+O(\epsilon^4), \tag{47}$$

where ϵ is the same small parameter as in expansions (14)–(16). Substituting Eq. (47) into the system (35)–(38), we find an exact solution at order ϵ: $u_+^{(1)}=u_-^{(1)}=u_{22}(r)$, where $u_{22}(r)$ solves the Eq. (21). At order ϵ^2, we need to solve the nonhomogeneous equation for $w_+^{(2)}(r)$,

$$w_+^{(2)\prime\prime}+\frac{1}{r}w_+^{(2)\prime\prime}-\left(\lambda_0+\frac{1}{r^2}\right)w_+^{(2)}+\frac{u_0^2}{1+su_0^2}w_+^{(2)}$$
$$=(\lambda_2-i\sigma_2)\phi-\frac{2\phi(u_0u_{20}+u_0u_{22}+\phi^2)}{(1+su_0^2)^2}. \tag{48}$$

The solvability condition for this equation can be simplified by the virtue of Eq. (28), and we find that the eigenvalue coefficient σ_2 is given as

$$\sigma_2=2i\frac{\int_0^\infty r\phi^2 h_2\,dr}{\int_0^\infty r\phi^2\,dr}. \tag{49}$$

Utilizing Eq. (32), we see that

$$\sigma_2=2i[2\lambda_{2d}(s)-\lambda_{2v}(s)], \tag{50}$$

whose imaginary part is positive from Fig. 1(a). Thus, the energy quadratic form of the bifurcated eigenmodes (47) and (50) (up to the order ϵ^2) is negative:

$$h=-\epsilon^2\mathrm{Im}(\sigma_2)\int_0^\infty r\phi^2\,dr<0. \tag{51}$$

The analytical eigenvalue formulas (47) and (50) at $n=2$ is plotted in Fig. 4 versus λ for $s=0.5$ (dash-dotted line). Numerically, we have determined these eigenvalues for $s=0.5$ and various values of λ, and the results are plotted in Fig. 4 (solid line) as well. When λ is close to λ_0, the analytical formula agrees well with the numerical values.

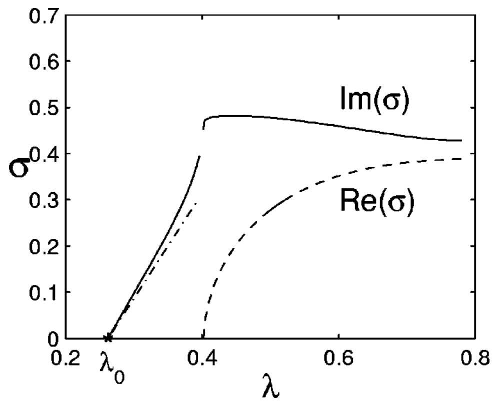

FIG. 4. Eigenvalues σ of vortex solitons versus λ at $s=0.5$ and $n=2$. The cutoff frequency λ_0 is marked by (*). Solid line: Im(σ); dashed line: Re(σ); dash-dotted line: analytical formulas (47) and (50).

We have shown above that the two zero eigenvalues of the system (42) at $n=\pm 2$ move to the imaginary axis when $\lambda>\lambda_0(s)$, while the two nonzero negative-energy eigenvalues at $n=\pm 1$ remain on the imaginary axis. Thus, we conclude that vortex solitons are linearly stable near the cutoff frequency $\lambda=\lambda_0(s)$, i.e., vortex solitons with small vortex components are linearly stable. This result confirms the conclusions of Ref. [20] and does not support conclusions of Ref. [23], where *all* vortex vector solitons were claimed to be linearly unstable.

Unstable eigenvalues of vortex solitons may appear far away from the cutoff frequency $\lambda_0(s)$. Indeed, the two imaginary eigenvalues σ for $n=\pm 2$ that bifurcate from zero eigenvalues at $\lambda>\lambda_0(s)$ have negative energy (51). When these eigenvalues collide with eigenvalues of positive energy or with continuous spectrum, the oscillatory instability may arise [35,38]. We confirm this scenario and compute unstable eigenvalues σ of the linear systems (35)–(38) with the numerical shooting method. The unstable eigenvalues are found exactly at $n=\pm 2$ and are shown in Fig. 4 for $s=0.5$. The unstable eigenvalues appear when $\lambda>\lambda_c\approx 0.402$, where λ_c denotes the frequency for onset of instability. These results agree with Fig. 3 of Ref. [23], where the unstable eigenvalues were found from time integration of the linearized equations under random-noise initial perturbations. Figure 5 displays our numerical solutions for the vortex soliton and the corresponding unstable eigenfunction at $s=0.5$, $\lambda=0.5$, and $n=2$. Thus, for the case $s=0.5$, unstable eigenvalues exist at $\lambda>\lambda_c\approx 0.402$, while vortex vector solitons exist at $\lambda>\lambda_0\approx 0.2622$, see Fig. 4. In the interval $\lambda_0<\lambda<\lambda_c$, i.e., $0.2622<\lambda<0.402$ for $s=0.5$, unstable eigenvalues do not exist and the vortex solitons are linearly *stable*.

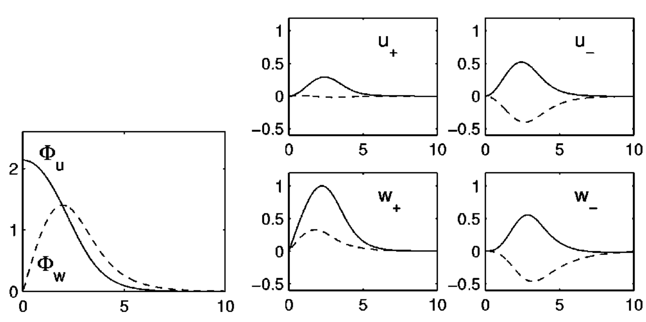

FIG. 5. The vortex soliton (left) and its unstable eigenmode (right) at $s=0.5$, $\lambda=0.5$, and $n=2$. In the right figure, solid lines are the real parts of the eigenfunctions, and dashed lines are the imaginary parts.

We conclude this analysis with two remarks. First, it follows from Fig. 4 for $s=0.5$ that the eigenvalues σ at $n=\pm 2$ merge into the continuous spectrum at $\lambda\approx 0.396$, while unstable eigenvalues appear at $\lambda=\lambda_c\approx 0.402$. Our numerical results are inconclusive as to what happens in the narrow interval $0.396<\lambda<0.402$. This problem is left open for future studies. And second, when λ is further away from the cutoff frequency $\lambda_0(s)$, the vector vortex solution bifurcates into scalar vortex solutions with $u=0$ and $w=\Phi_w(r)e^{i\theta}$, see Ref. [28]. The scalar vortex soliton has additional unstable eigenmodes at $|n|\neq 2$ that have smaller growth rates (see Ref. [15]). We do not study this bifurcation, where the family of vector vortex solitons terminates, nor the number of unstable eigenvalues of vector vortex solitons near this bifurcation.

B. Dipole soliton

To study the linear stability of the dipole solitons (8), we linearize the system (1) and (2) with the perturbation,

$$E_1=e^{iz}\{U(x,y)+[u_r(x,y)+u_i(x,y)]e^{\sigma z}+[\overline{u_r}(x,y)-\overline{u_i}(x,y)]e^{\bar{\sigma}z}\},\tag{52}$$

$$E_2=e^{i\lambda z}\{W(x,y)+[w_r(x,y)+w_i(x,y)]e^{\sigma z}+[\overline{w_r}(x,y)-\overline{w_i}(x,y)]e^{\bar{\sigma}z}\}.\tag{53}$$

Here, u_r, u_i, w_r, and w_i are complex functions and are very small. The linearization problem is then written in the form

$$i\sigma u_i=-\Delta u_r+u_r-(V+2V_{uu})u_r-2V_{uw}w_r,\tag{54}$$

$$i\sigma u_r=-\Delta u_i+u_i-Vu_i,\tag{55}$$

$$i\sigma w_i=-\Delta w_r+\lambda w_r-(V+2V_{ww})w_r-2V_{uw}u_r,\tag{56}$$

$$i\sigma w_r=-\Delta w_i+\lambda w_i-Vw_i,\tag{57}$$

where

$$V=\frac{U^2+W^2}{1+s(U^2+W^2)},\quad V_{uu}=\frac{U^2}{[1+s(U^2+W^2)]^2},$$

$$V_{uw}=\frac{UW}{[1+s(U^2+W^2)]^2},\quad V_{ww}=\frac{W^2}{[1+s(U^2+W^2)]^2}.$$

The linearized problem can be formulated in the same Hamiltonian form (39) with the energy quadratic form [38]

$$h=i\sigma\int_{-\infty}^{\infty}\int_{-\infty}^{\infty}(\bar{u}_r u_i+\bar{u}_i u_r+\bar{w}_r w_i+\bar{w}_i w_r)dxdy. \quad (58)$$

At the cutoff frequency $\lambda=\lambda_0(s)$, the same analysis, as for the vortex solitons, shows existence of a pair of eigenvalues $\sigma=\pm i(1-\lambda_0)$ with negative values of h and a number of zero eigenvalues with zero values of h. We show again that the eigenvalues $\sigma=\pm i(1-\lambda_0)$ with negative energy never bifurcate into a complex domain for $\lambda>\lambda_0(s)$. Indeed, for any value of λ, the linearization problems (54)–(57) have the exact solution

$$u_r=-W(x,y),\quad u_i=W(x,y),\quad w_r=U(x,y),\quad w_i=U(x,y) \quad (59)$$

at $\sigma=i(1-\lambda)$, and

$$u_r=W(x,y),\quad u_i=W(x,y),\quad w_r=-U(x,y),\quad w_i=U(x,y) \quad (60)$$

at $\sigma=-i(1-\lambda)$.

We study the zero eigenvalues of the systems (54)–(57) with perturbation series expansions for $\lambda>\lambda_0(s)$:

$$\sigma=\epsilon^2\sigma_2+O(\epsilon^4),\quad u_r=\epsilon u_r^{(1)}(r,\theta)+O(\epsilon^3),\quad u_i=O(\epsilon^3),$$
$$w_r=w_r^{(0)}(r,\theta)+\epsilon^2 w_r^{(2)}(r,\theta)+O(\epsilon^4),$$
$$w_i=w_i^{(0)}(r,\theta)+\epsilon^2 w_i^{(2)}(r,\theta)+O(\epsilon^4). \quad (61)$$

Here ϵ is the same small parameter as in expansions (14)–(16), while the functions $w_{r,i}^{(0)}(r,\theta)$ are linear combinations of the eigenfunctions of the null space of the problem (54)–(57) at $\lambda=\lambda_0(s)$:

$$w_r^{(0)}=c_1\phi(r)\cos\theta+c_2\phi(r)\sin\theta,$$
$$w_i^{(0)}=d_1\phi(r)\cos\theta+d_2\phi(r)\sin\theta, \quad (62)$$

where c_1, c_2, d_1, and d_2 are constants. Substituting Eq. (61) into the system (54)–(57), we find an exact solution at order ϵ,

$$u_r^{(1)}=c_1u_{20}(r)+(c_1\cos 2\theta+c_2\sin 2\theta)u_{22}(r), \quad (63)$$

where $u_{20}(r)$ and $u_{22}(r)$ solve the problems (20) and (21). At order ϵ^2, four solvability conditions are needed for solving the nonhomogeneous equations for $w_r^{(2)}(r,\theta)$ and $w_i^{(2)}(r,\theta)$. Using Eq. (30), we transform the four solvability conditions to the form

$$\sigma_2c_1=0,\quad \sigma_2d_2=0,\quad i\sigma_2c_2\int_0^\infty r\phi^2dr=d_2\int_0^\infty r\phi^2h_2dr,$$
$$i\sigma_2d_1\int_0^\infty r\phi^2dr=-c_1\int_0^\infty r\phi^2(2h_1+h_2)dr. \quad (64)$$

If $\sigma_2=0$ then $c_1=d_2=0$, while c_2, d_1 are arbitrary constants. Thus, the zero eigenvalue persists in the systems (54)–(57) for $\lambda>\lambda_0(s)$ with two eigenfunctions $w_r=\phi(r)\sin\theta$ and $w_i=\phi(r)\cos\theta$. The two eigenfunctions are related to the symmetries of the systems (1) and (2) with respect to rotation in θ and shift of the complex phase. If $\sigma_2\neq 0$, however, the system (64) has only the trivial solution: $c_1=c_2=d_1=d_2=0$. Therefore, the other two zero eigenvalues do not bifurcate to the imaginary axis but simply disappear for $\lambda>\lambda_0(s)$.

We have analytically proved above that the dipole solitons are linearly stable in the neighborhood of the cutoff frequency $\lambda_0(s)$. Moreover, contrary to vortex solitons, there are only two eigenvalues of negative energy for $\lambda>\lambda_0(s)$, and they remain on the imaginary axis for all values of λ [see Eqs. (59) and (60)]. Thus, we conjecture that the dipole solitons are linearly stable in the whole domain of their existence. This conjecture is in agreement with the numerical work in Ref. [23]. We again confirm this result by numerical simulations of the systems (1) and (2) linearized around the dipole soliton (8). For $s=0.5$, we have simulated the linearized system for several values of λ between $\lambda=0.3$ and $\lambda=0.85$. We did not find any instability in the linearized system. Since $\lambda=0.3$ is close to the cutoff frequency $\lambda_0=0.2622$ and $\lambda=0.85$ is close to the end frequency $\lambda=1$, we conclude that dipole solitons are indeed linearly *stable* in the whole existence interval.

IV. NONLINEAR EVOLUTION OF PERTURBED VORTEX SOLITONS

Here, we study the nonlinear evolution of perturbed vortex solitons. The unstable vortex soliton under small random-noise perturbations was found in Ref. [23] to break up into a rotating dipole vector soliton. We will show below that such a breakup scenario holds only when the vortex component of the vortex soliton is below a certain threshold. Above that threshold, unstable vortex solitons break up into two rotating fundamental vector solitons instead. We will also show that the vortex solitons with small vortex components are not only linearly stable but also nonlinearly stable.

We consider first the nonlinear evolution of linearly stable vortex solitons. For this purpose, we have simulated the system (1) and (2) starting with a linearly stable vortex soliton under various types of small initial perturbations such as random-noise and amplitude scaling. We have found that the vortex solitons are also nonlinearly stable for all small perturbations. To demonstrate, we select $s=0.5$ and $\lambda=0.38$, where the vortex soliton has been shown to be linearly stable (see Fig. 4). As initial perturbations, we chose

$$E_1(r,\theta,0)=(1+\alpha)\Phi_u(r,\lambda),$$
$$E_2(r,\theta,0)=(1+\alpha)\Phi_w(r,\lambda)e^{i\theta}, \quad (65)$$

where α is a small perturbation parameter that measures amplification of the vortex soliton by a factor $1+\alpha$. The simulation result with $\alpha=0.05$ is shown in Fig. 6. This figure shows that the perturbed vortex soliton persists the nonlinear evolution and exhibits little change of shape even after 300 diffraction lengths. This clearly confirms the linear and non-

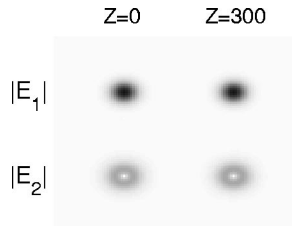

FIG. 6. Stable evolution of vortex vector solitons with $\lambda<\lambda_c$ under the perturbation (65) with $s=0.5$, $\lambda=0.38$, and $\alpha=0.05$.

linear stabilities of the vortex soliton with $s=0.5$ and $\lambda=0.38$. Other perturbations to this soliton give similar evolution results.

We study next the nonlinear evolution of linearly unstable vortex solitons. We have shown in Sec. III A that these solitons possess two unstable eigenmodes $(\sigma,n,u_+,u_-,w_+,w_-)$ and $(\bar{\sigma},-n,\bar{u}_-,\bar{u}_+,\bar{w}_-,\bar{w}_+)$ with $n=2$. The σ versus λ graph is shown in Fig. 4 for $s=0.5$, while unstable eigenfunctions (u_+,u_-,w_+,w_-) for $s=0.5$ and $\lambda=0.5$ are displayed in Fig. 5. However, we recognize that these two unstable eigenmodes are equivalent in view of Eqs. (33) and (34). Thus, any small initial perturbation to the vortex soliton is projected onto this unstable eigenmode, which grows exponentially, while the rest of the initial perturbation disperses away. For convenience, we choose the initial perturbation to be exactly this unstable eigenmode, i.e.,

$$E_1(r,\theta,0)=\Phi_u(r)+\alpha[u_+(r)e^{-2i\theta}+\bar{u}_-(r)e^{2i\theta}], \quad (66)$$

$$E_2(r,\theta,0)=e^{i\theta}\{\Phi_w(r)+\alpha[w_+(r)e^{-2i\theta}+\bar{w}_-(r)e^{2i\theta}]\}, \quad (67)$$

where α is a small perturbation parameter. The advantage of this special perturbation is that it shortens the distance for the breakup of the vortex soliton and reduces the radiation noise in the nonlinear evolution of the perturbed solution.

We have discovered two breakup scenarios of the unstable vortex soliton with the initial perturbations (66) and (67). We confirm that the unstable vortex solitons with relatively *small* vortex components indeed break up into a rotating dipole soliton, in agreement with Ref. [23]. However, when the vortex component increases above a certain threshold, an unstable vortex soliton breaks up into two rotating *fundamental* vector solitons rather than one dipole soliton. For example, when $s=0.5$ and $\alpha=0.05$, the vortex soliton breaks up into a dipole soliton when $0.402<\lambda\lesssim 0.45$, and into two fundamental vector solitons when $\lambda>0.45$. Indeed, when $\lambda=0.45$ (where the vortex component is relatively small), the time evolution of the perturbed vortex soliton is plotted in Fig. 7. It is seen that this soliton breaks up into a rotating dipole soliton. But when $\lambda=0.5$ (where the vortex component is bigger), the time evolution is shown in Fig. 8. Here, two rotating fundamental vector solitons are formed after the breakup of the unstable vortex soliton. We have also found that these breakup scenarios are insensitive to the type of initial perturbation imposed because we have simulated the evolutions with different values of α in Eqs. (66) and (67) as well as with other forms of initial perturbations such as random noise, but the breakup scenarios do not change. To check the numerical accuracy of our simulations, we have used more grid points and wider (x,y) intervals and obtained identical results. Furthermore, our results conserve energies of the E_1 and E_2 components very well.

FIG. 7. Breakup of an unstable vortex soliton into a rotating dipole soliton under the perturbations (66) and (67) with $s=0.5$, $\lambda=0.45$, and $\alpha=0.05$.

Intuitively, it is not difficult to understand the above two breakup scenarios of unstable vortex solitons. When the vortex component of the vortex soliton is small, the instability (with $n=2$) breaks up the vortex (E_2) component into two weak humps, while it does not significantly affect the single-hump shape of the fundamental (E_1) component since E_1's initial amplitude is much higher. During the subsequent evolution, the two humps of the E_2 component are too weak to break the E_1 component into two pieces, thus the solution relaxes into a dipole soliton instead of two fundamental solitons. However, when the vortex component of the vortex soliton is sufficiently large, the fundamental component becomes small (see Fig. 2 and Ref. [23]). In this case, instability breaks up both the vortex and fundamental components into two pieces, and two fundamental solitons are formed then.

V. SUMMARY AND DISCUSSION

To summarize, we have studied both analytically and numerically the existence, uniqueness, and stability of vortex and dipole vector solitons in saturable optical materials in $(2+1)$ dimensions. We have shown that the analytical expressions for vortex and dipole vector solitons can be constructed with perturbation series expansions near the cutoff frequency $\lambda=\lambda_0(s)$. We have also shown that only two vector solitons bifurcate from the same cutoff frequency, which

FIG. 8. Breakup of an unstable vortex soliton into two fundamental solitons under the perturbations (66) and (67) with $s=0.5$, $\lambda=0.5$, and $\alpha=0.05$.

are vortex and dipole solitons. Furthermore, we have proved that both vortex and dipole solitons are linearly *stable* when the vortex and dipole components are *small*. As the vortex and dipole components increase, the family of vortex vector solitons becomes linearly unstable, while that of dipole vector solitons remains linearly stable in the entire existence domain. We have also shown that unstable vortex solitons break up into a rotating dipole soliton only when the vortex component is relatively small. When the vortex component crosses a certain threshold, the vortex soliton breaks up into two rotating fundamental vector solitons instead. We expect that our results are significant not only for studies of spatial vector solitons in a saturable nonlinear medium but also for studies of Bose-Einstein condensation.

In this paper, we have studied only the simplest vortex and dipole vector solitons that bifurcate from the fundamental u and small w components. One natural question to ask is about the existence and stability of other vortex and multipole vector solitons. The perturbation series expansion method developed in this paper is powerful for a systematic study of general vortex and multipole vector solitons near their bifurcation points. But this problem lies outside the scope of the present article. We note, however, that vortex solitons (7) with $|n|>0$ and $|m|>0$ exist, and they are expected to be always linearly unstable because each component has nonzero charge and is linearly unstable by itself [15]. This expectation is consistent with our preliminary numerical simulations on vortex solitons with charges such as $n=1$ and $m=-1$.

Recently, three-component vortex and dipole vector solitons in a saturable medium have been investigated [39]. The authors found that those solitons are linearly unstable provided that their total topological charge is nonzero. In view of our results in this paper, this conclusion needs modification. We plan to study this system carefully in the near future.

ACKNOWLEDGMENTS

The authors appreciate helpful discussions with Yu. Kivshar, Z. Musslimani, B. Sandstede, and D. Skryabin. The work of D.P. was supported in part by the NSERC, Grant No. 5-36694, and CFI, Grant No. 5-26773. The work of J.Y. was supported in part by the Air Force Office of Scientific Research under Contract No. F49620-99-1-0174 and by the National Science Foundation under Grant No. DMS-9971712.

[1] R.Y. Chiao, E. Garmire, and C.H. Townes, Phys. Rev. Lett. **13**, 479 (1964).
[2] *Spatial Solitons*, edited by S. Trillo and W. Torruellas (Springer-Verlag, Berlin, 2001).
[3] V.E. Zakharov and A.B. Shabat, Zh. Éksp. Teor. Fiz. **61**, 118 (1971) [Sov. Phys. JETP **34**, 62 (1972)].
[4] A. Barthelemy, S. Maneuf, and C. Froehly, Opt. Commun. **55**, 201 (1985).
[5] J.S. Aitchison, A.M. Weiner, Y. Silberberg, M.K. Oliver, J.I. Jackel, D.E. Learird, E.M. Vogel, and P.W.E. Smith, Opt. Lett. **15**, 471 (1990).
[6] V.E. Zakharov, Zh. Éksp. Theor. Fiz. **18**, 1745 (1972) [Sov. Phys. JETP **35**, 908 (1972)].
[7] L. Berge, Phys. Rep. **303**, 259 (1998).
[8] G.I. Stegeman and M. Segev, Science **286**, 1518 (1999).
[9] J.M. Soto-Crespo, E.M. Wright, and N.N. Akhmediev, Phys. Rev. A **45**, 3168 (1992).
[10] D.E. Edmundson and R.H. Enns, Opt. Lett. **17**, 586 (1992); **18**, 1609 (1993); Phys. Rev. A **51**, 2491 (1995).
[11] M. Mitchell, M. Segev, and D.N. Christodoulides, Phys. Rev. Lett. **80**, 4657 (1998).
[12] J.W. Grantham, H.M. Gibbs, G. Khitrova, J.F. Valley, and J. Xu, Phys. Rev. Lett. **66**, 1422 (1991).
[13] D.E. Edmundson, Phys. Rev. E **55**, 7636 (1997).
[14] N. N. Akhmediev and A. Ankiewicz, *Solitons* (Chapman and Hall, London, 1997).
[15] W.J. Firth and D.V. Skryabin, Phys. Rev. Lett. **79**, 2450 (1997).
[16] J. Yang, Phys. Rev. E **66**, 026601 (2002).
[17] N.N. Rosanov, S.V. Fedorov, N.A. Kaliteevskii, D.A. Kirsanov, P.I. Krepostnov, and V.O. Popov, Nonlinear Opt. **23**, 21 (2000).
[18] C. Anastassiou, M. Segev, K. Steiglitz, J.A. Giordmaine, M. Mitchell, M. Shih, S. Lan, and J. Martin, Phys. Rev. Lett. **83**, 2332 (1999).
[19] A.V. Buryak, Y.S. Kivshar, M. Shih, and M. Segev, Phys. Rev. Lett. **82**, 81 (1999).
[20] Z.H. Musslimani, M. Segev, D.N. Christodoulides, and M. Soljacic, Phys. Rev. Lett. **84**, 1164 (2000).
[21] Z.H. Musslimani, M. Segev, and D.N. Christodoulides, Opt. Lett. **25**, 61 (2000).
[22] J.N. Malmberg, A.H. Carlsson, D. Anderson, M. Lisak, E.A. Ostrovskaya, and Y.S. Kivshar, Opt. Lett. **25**, 643 (2000).
[23] J.J. Garcia-Ripoll, V.M. Perez-Garcia, E.A. Ostrovskaya, and Y.S. Kivshar, Phys. Rev. Lett. **85**, 82 (2000).
[24] T. Carmon, C. Anastassiou, S. Lan, D. Kip, Z.H. Musslimani, and M. Segev, Opt. Lett. **25**, 1113 (2000).
[25] W. Krolikowski, E.A. Ostrovskaya, C. Weilnau, M. Geisser, G. McCarthy, Y.S. Kivshar, C. Denz, and B. Luther-Davies, Phys. Rev. Lett. **85**, 1424 (2000).
[26] Z.H. Musslimani, M. Soljai, M. Segev, and D.N. Christodoulides, Phys. Rev. Lett. **86**, 799 (2001).
[27] Z.H. Musslimani, M. Soljacic, M. Segev, and D.N. Christodoulides, Phys. Rev. E **63**, 066608 (2001).
[28] A.S. Desyatnikov, D. Neshev, E.A. Ostrovskaya, Y.S. Kivshar, G. McCarthy, W. Krolikowski, and B. Luther-Davies, J. Opt. Soc. Am. B **19**, 586 (2002).
[29] C.R. Menyuk, IEEE J. Quantum Electron. **QE-23**, 174 (1987).
[30] G.P. Agrawal, *Nonlinear Fiber Optics* (Academic Press, San Diego, 1989).
[31] A. Hasegawa and Y. Kodama, *Solitons in Optical Communications* (Clarendon, Oxford, 1995).

[32] E.A. Ostrovskaya, Y.S. Kivshar, D.V. Skryabin, and W. Firth, Phys. Rev. Lett. **83**, 296 (1999).
[33] J. Yang, Physica D **108**, 92 (1997).
[34] J. Yang and Y. Tan, Phys. Rev. Lett. **85**, 3624 (2000).
[35] D.V. Skryabin, Phys. Rev. A **63**, 013602 (2001).
[36] D.E. Pelinovsky and J. Yang, Stud. Appl. Math. **105**, 245 (2000).
[37] D.E. Pelinovsky and Yu.S. Kivshar, Phys. Rev. E **62**, 8668 (2000).
[38] D.E. Pelinovsky (unpublished).
[39] A.S. Desyatnikov, Y.S. Kivshar, K. Motzek, F. Kaiser, C. Weilnau, and C. Denz, Opt. Lett. **27**, 634 (2002).